Chapter 5

Polarimetry with random light

5.1 Introduction

Polarization, a fundamental characteristic of light, is crucial in various applications such as imaging [159,375], remote sensing [376,377], communication [239], metrology [378], biological microscopy [267], plasmonics [379], quantum information technology [240], and so on [25]. Accurate measurement of the state of polarization (SOP) is therefore essential. Over the past century, Stokes polarimetry has been widely employed to measure the SOP [27,119,380]. Traditional techniques for full-Stokes polarimetry require at least four intensity measurements to calculate the four Stokes parameters (SPs) using various combinations of linear and circular polarization channels. These sequential measurements typically involve the mechanical rotation of optical elements such as quarter-wave plates (QWPs) and linear polarizers (LPs), which limit measurement speed and add errors. To overcome these limitations, recent advancements aim to achieve fast Stokes polarimetry by developing single-shot methods using new materials and other methods. These methods include multiple cameras [381], single polarization camera [120,121,123], digital micromirror devices (DMDs) [124,125], supervised learning [126], metasurfaces [122,127–130], etc. Among them, metasurface-based methods have provided a new dimension for real-time polarimetry, but the optical materials used for this purpose require special design and a specialized microfabrication process. In another approach, digital holography (DH) is utilized for polarization measurement by mixing the field with a controllable reference beam [139,382–387]. These techniques are largely confined to free space and homogeneous media.

Direct recovery of the SOP from the randomly scattered light is another challenging yet a practical issue [226]. This appears in many practical applications, such as biomedical imaging [290], endoscopy [388], adaptive optics [389], remote sensing [261], etc. Methods such as wavefront shaping [390,391], transmission matrix [392], and projection

on the Poincaré space [370–372] are developed to suppress the random light and retrieve the desired SOP. The wavefront shaping technique first detects the distorted wavefront of the polarization components of random light and then corrects it to retrieve the desired SOP. In contrast, the transmission matrix uses a linear relation between the SOP of the incident and the randomly scattered pattern. On the other hand, correlation techniques utilize randomness for information recovery, including the SOPs. For instance, the SOP of the randomly scattered incident beam is recovered from two-point correlations of the vector field [393]. Specifically, the two-point complex coherence functions between the same and orthogonal polarization components recover the SOP of the incident beam from intensity correlations [211,212,215,216]. In this context, generalized Stokes parameters (GSPs), an extension of SPs from one-point to two-point quantities, have been pivotal in advancing characterization and imaging techniques [194,218,221,273]. Recent focus on GSPs has led to the development of Stokes holography. This technique retrieves the SOP of polarized objects hidden behind the random scattering medium by utilizing field and intensity correlations of the vector field [134,222]. In these techniques, object information is encoded into the Stokes fringes and reconstructed as a distribution of the GSPs. Additionally, the polarization correlations of the vector field are applied to characterize the vector beams [223,285], polarization dynamics [280], ghost polarimetry [394], etc. These methods have further advanced holography techniques by reconstructing complex GSPs, thereby enabling the extraction of polarization information obscured within scattering media [238,268,369]. Despite these advances, existing methods rely on multiple measurements and require rotated polarization elements, hindering efficient and real-time SOP measurement.

In this chapter, we present and experimentally demonstrate a new technique for single-shot full-Stokes polarimetry. This is achieved by inserting a diffuser in the beam's path

and recording the orthogonal polarization components of randomly scattered light in a single-intensity frame using a tuneable beam displacer. This technique leverages the randomness introduced by the diffuser to extract the two-point complex GSPs of the randomly scattered field, which are then used to retrieve the SPs of the incident beam. The experimental methodology of the proposed technique begins with the determination of two SPs, namely $S_0(\boldsymbol{r})$ and $S_1(\boldsymbol{r})$ from the recorded intensity pattern of the randomly scattered light. The two-point Stokes correlation functions of these two SPs is calculated, followed by Fourier fringe analysis, to measure the two-point complex GSPs. A relation is established between the complex GSPs and the incident beam's SPs before the diffuser. This process enables the determination of all four SPs of the incident beam. The following discussion includes a thorough theoretical justification and the associated experimental studies.

5.2 Theoretical basis

Consider a coherent beam propagating along the *z*-direction. The instantaneous complex field at a time *t* and a position vector ρ at the source plane *z*=0 is represented as

$$\boldsymbol{U}(\boldsymbol{\rho},t) = U_x(\boldsymbol{\rho},t)\hat{x} + U_y(\boldsymbol{\rho},t)\hat{y}\,, \tag{5.1}$$

where, $\hat{x}$ and $\hat{y}$ are the unit vectors along the horizontal and vertical directions, respectively. For a coherent beam, time *t* is ignored from further consideration in the coming sections, and the SPs are represented as

$$S_n(\boldsymbol{\rho}) = \sum_{a,b} U_a^*(\boldsymbol{\rho})\sigma_{ab}^n U_b(\boldsymbol{\rho}), \qquad (a,b=x,y) \tag{5.2}$$

where *n*=0-3, asterisk * indicates the complex conjugate and σ represents Pauli spin matrices. When a polarized coherent beam travels through a diffuser, the scattered field at

the observation plane, as shown in Fig. 5.1, is related to the incident polarized beam as follows

$$U_a(\boldsymbol{r}) = U_a(\boldsymbol{\rho}) \otimes h(\boldsymbol{r} - \boldsymbol{\rho}), \tag{5.3}$$

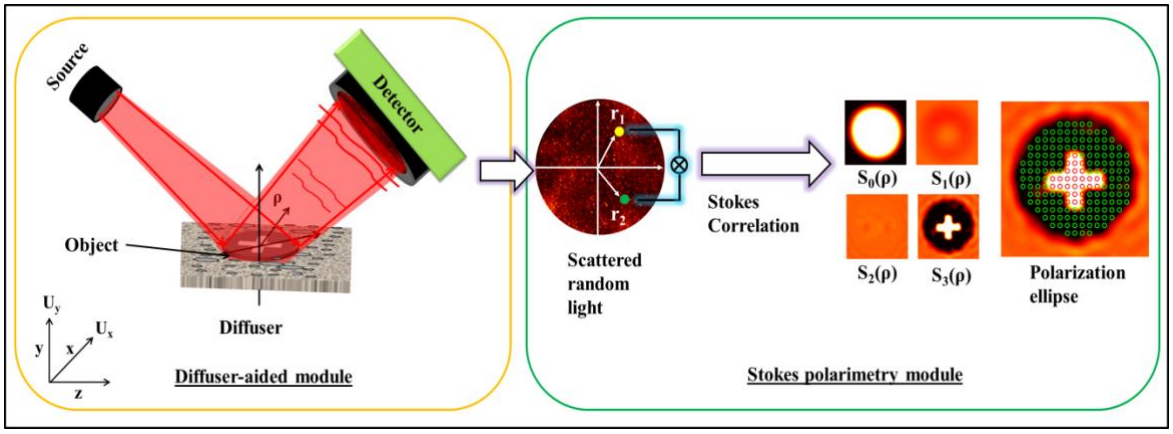

Fig. 5.1 Conceptual representation of the proposed technique.

where, $\otimes$ represents the convolution, $U_a(\boldsymbol{\rho}) = e^{i\phi(\rho)}U_a(\boldsymbol{\rho})$, i.e. the random phase $\phi(\boldsymbol{\rho})$ introduced by the scattering media is embedded in $U_a(\boldsymbol{\rho})$, $h(\boldsymbol{r} - \boldsymbol{\rho}) = \frac{e^{ikz}}{i\lambda z}\exp\left[\frac{ik}{2z}(\boldsymbol{r} - \boldsymbol{\rho})^2\right]$ is the propagation kernel, $\boldsymbol{r}$ is the position vector at the observation plane respectively, and λ is the wavelength of the light. The constant phase term $\frac{e^{ikz}}{i\lambda z}$ is ignored from further consideration as we are interested in observations at a fixed z value.

The two-point correlation characterizes the random field, and we select the GSPs to characterize the random field as follows

$$S_n(\boldsymbol{r_1}, \boldsymbol{r_2}) = \sum_{a,b}\left\langle U_a^*(\boldsymbol{r_1})\sigma_{ab}^n U_b(\boldsymbol{r_2})\right\rangle, \tag{5.4}$$

where, $S_n(\boldsymbol{r_1},\boldsymbol{r_2})$, a two-point extension of the SPs, are GSPs and $\langle\ \rangle$ denotes the ensemble average. The GSPs are complex quantities compared to the SPs.

The correlations of fluctuations of the SPs of the random field are leveraged to build a polarimeter. The fluctuations of SPs of the random field with respect to their average value are defined as

$$\Delta S_n(\boldsymbol{r}) = S_n(\boldsymbol{r}) - \langle S_n(\boldsymbol{r})\rangle, \tag{5.5}$$

where, $\langle S_n(\boldsymbol{r})\rangle$ is the average of the SPs.

All possible pairs of the two-point correlations between the various fluctuations of SPs are described using a 4 × 4 matrix as follows,

$$C_{nm}(\boldsymbol{r_1},\boldsymbol{r_2}) = \langle \Delta S_n(\boldsymbol{r_1})\Delta S_m(\boldsymbol{r_2})\rangle, \qquad n, m=0\text{-}3 \tag{5.6}$$

Out of sixteen Stokes correlations in Eq. (5.6), we used only four to extract the GSPs as follows

$$C_{00}(\boldsymbol{r_1},\boldsymbol{r_2}) = \frac{1}{2}\left[|S_0(\boldsymbol{r_1},\boldsymbol{r_2})|^2 + |S_1(\boldsymbol{r_1},\boldsymbol{r_2})|^2 + |S_2(\boldsymbol{r_1},\boldsymbol{r_2})|^2 + |S_3(\boldsymbol{r_1},\boldsymbol{r_2})|^2\right], \tag{5.7}$$

$$C_{01}(\boldsymbol{r_1},\boldsymbol{r_2}) = \mathrm{Re}\left(S_0(\boldsymbol{r_1},\boldsymbol{r_2})S_1^*(\boldsymbol{r_1},\boldsymbol{r_2})\right) - \mathrm{Im}\left(S_2(\boldsymbol{r_1},\boldsymbol{r_2})S_3^*(\boldsymbol{r_1},\boldsymbol{r_2})\right), \tag{5.8}$$

$$C_{10}(\boldsymbol{r_1},\boldsymbol{r_2}) = \mathrm{Re}\left(S_0(\boldsymbol{r_1},\boldsymbol{r_2})S_1^*(\boldsymbol{r_1},\boldsymbol{r_2})\right) + \mathrm{Im}\left(S_2(\boldsymbol{r_1},\boldsymbol{r_2})S_3^*(\boldsymbol{r_1},\boldsymbol{r_2})\right), \tag{5.9}$$

$$C_{11}(\boldsymbol{r_1},\boldsymbol{r_2}) = \frac{1}{2}\left[|S_0(\boldsymbol{r_1},\boldsymbol{r_2})|^2 + |S_1(\boldsymbol{r_1},\boldsymbol{r_2})|^2 - |S_2(\boldsymbol{r_1},\boldsymbol{r_2})|^2 - |S_3(\boldsymbol{r_1},\boldsymbol{r_2})|^2\right], \tag{5.10}$$

Eqs. (5.7)-(5.10) are utilized to extract the GSPs as follows,

$$A(\boldsymbol{r_1},\boldsymbol{r_2}) = \frac{1}{4}\left[\left(C_{00}(\boldsymbol{r_1},\boldsymbol{r_2}) + C_{11}(\boldsymbol{r_1},\boldsymbol{r_2})\right) + \left(C_{10}(\boldsymbol{r_1},\boldsymbol{r_2}) + C_{01}(\boldsymbol{r_1},\boldsymbol{r_2})\right)\right] = \frac{1}{4}|S_0(\boldsymbol{r_1},\boldsymbol{r_2}) + S_1(\boldsymbol{r_1},\boldsymbol{r_2})|^2, \tag{5.11}$$

$$B(\boldsymbol{r_1},\boldsymbol{r_2})=\frac{1}{4}\Big[\big(C_{00}(\boldsymbol{r_1},\boldsymbol{r_2})+C_{11}(\boldsymbol{r_1},\boldsymbol{r_2})\big)-\big(C_{10}(\boldsymbol{r_1},\boldsymbol{r_2})+C_{01}(\boldsymbol{r_1},\boldsymbol{r_2})\big)\Big]=\frac{1}{4}\big|S_0(\boldsymbol{r_1},\boldsymbol{r_2})-S_1(\boldsymbol{r_1},\boldsymbol{r_2})\big|^2,$$

(5.12)

$$C(\boldsymbol{r_1},\boldsymbol{r_2})=\frac{1}{4}\Big[\big(C_{00}(\boldsymbol{r_1},\boldsymbol{r_2})-C_{11}(\boldsymbol{r_1},\boldsymbol{r_2})\big)+\big(C_{10}(\boldsymbol{r_1},\boldsymbol{r_2})-C_{01}(\boldsymbol{r_1},\boldsymbol{r_2})\big)\Big]=\frac{1}{4}\big|S_2(\boldsymbol{r_1},\boldsymbol{r_2})+iS_3(\boldsymbol{r_1},\boldsymbol{r_2})\big|^2,$$

(5.13)

$$D(\boldsymbol{r_1},\boldsymbol{r_2})=\frac{1}{4}\Big[\big(C_{00}(\boldsymbol{r_1},\boldsymbol{r_2})-C_{11}(\boldsymbol{r_1},\boldsymbol{r_2})\big)-\big(C_{10}(\boldsymbol{r_1},\boldsymbol{r_2})-C_{01}(\boldsymbol{r_1},\boldsymbol{r_2})\big)\Big]=\frac{1}{4}\big|S_2(\boldsymbol{r_1},\boldsymbol{r_2})-iS_3(\boldsymbol{r_1},\boldsymbol{r_2})\big|^2,$$

(5.14)

where, $A(\boldsymbol{r_1},\boldsymbol{r_2}),B(\boldsymbol{r_1},\boldsymbol{r_2}),C(\boldsymbol{r_1},\boldsymbol{r_2}),D(\boldsymbol{r_1},\boldsymbol{r_2})$ represents different combinations of four correlation functions i.e. Eqs. (5.7-5.10) to extract the GSPs. However, Eqs. (5.11)-(5.14) reconstruct only the modulus part of the GSPs, and the phase is lost. To extract the polarimetric parameters of the source from its random field, we need to measure the complex GSPs and then apply the inverse Fourier transform to get the polarimetric parameters of the source. Here, we propose a holographic approach with the higher-order SPs correlation and recover the complex GSPs. This is implemented by considering the SPs at the observation plane as a superposition of two SPs, i.e. from two independent sources as

$$S_n(\boldsymbol{r})=S_n^O(\boldsymbol{r})+S_n^R(\boldsymbol{r}),\tag{5.15}$$

where $S_n^O(\boldsymbol{r})$ and $S_n^R(\boldsymbol{r})$ are SPs of the unknown and known fields, respectively.

Therefore, the correlations of the fluctuations of SPs are represented as

$$\left\langle \Delta S_n(\boldsymbol{r_1})\Delta S_m(\boldsymbol{r_2})\right\rangle=\left\langle \Delta S_n^O(\boldsymbol{r_1})\Delta S_m^O(\boldsymbol{r_2})\right\rangle+\left\langle \Delta S_n^R(\boldsymbol{r_1})\Delta S_m^R(\boldsymbol{r_2})\right\rangle\tag{5.16}$$

as $\left\langle S_n^O(\boldsymbol{r_1})S_n^R(\boldsymbol{r_2})\right\rangle\approx 0$, due to statistically independent fields in Eq. (5.15).

Hence, the right-hand side of Eqs. (5.11)-(5.14) transforms to

$$\left|S_n(\boldsymbol{r_1},\boldsymbol{r_2})\right|^2 = \left|S_n^O(\boldsymbol{r_1},\boldsymbol{r_2}) + S_n^R(\boldsymbol{r_1},\boldsymbol{r_2})\right|^2 \tag{5.17}$$

where, $S_n^O(\boldsymbol{r_1},\boldsymbol{r_2}) = \sum_{a,b}\left\langle U_a^{O*}(\boldsymbol{r_1})\sigma_{ab}^n U_b^O(\boldsymbol{r_2})\right\rangle$, and $S_n^R(\boldsymbol{r_1},\boldsymbol{r_2}) = \sum_{a,b}\left\langle U_a^{R*}(\boldsymbol{r_1})\sigma_{ab}^n U_b^R(\boldsymbol{r_2})\right\rangle$. Eq. (5.17) states that the complex GSPs can be recovered from the correlation of the SPs. The reference $S_n^R(\boldsymbol{r_1},\boldsymbol{r_2})$ is selected in such a way that it covers the support of the desired GSPs, i.e. $S_n^O(\boldsymbol{r_1},\boldsymbol{r_2})$ to record the fringes in the Stokes correlation.

Fourier transforms of the Stokes correlation fringes generate three spectra: (i) object spectra, (ii) its conjugate, and (iii) a DC term. The object spectrum is filtered and translated to the origin at the Fourier plane. The inverse Fourier transform of the centrally shifted spectrum and its appropriate combinations provide the desired GSPs of the source as follows

$$S_0^O(\boldsymbol{r_1},\boldsymbol{r_2}) = a(\boldsymbol{r_1},\boldsymbol{r_2}) + b(\boldsymbol{r_1},\boldsymbol{r_2}), \tag{5.18}$$

$$S_1^O(\boldsymbol{r_1},\boldsymbol{r_2}) = a(\boldsymbol{r_1},\boldsymbol{r_2}) - b(\boldsymbol{r_1},\boldsymbol{r_2}), \tag{5.19}$$

$$S_2^O(\boldsymbol{r_1},\boldsymbol{r_2}) = c(\boldsymbol{r_1},\boldsymbol{r_2}) + d(\boldsymbol{r_1},\boldsymbol{r_2}), \tag{5.20}$$

$$S_3^O(\boldsymbol{r_1},\boldsymbol{r_2}) = i\left(d(\boldsymbol{r_1},\boldsymbol{r_2}) - c(\boldsymbol{r_1},\boldsymbol{r_2})\right) \tag{5.21}$$

where, $a(\boldsymbol{r_1},\boldsymbol{r_2}), b(\boldsymbol{r_1},\boldsymbol{r_2}), c(\boldsymbol{r_1},\boldsymbol{r_2}), d(\boldsymbol{r_1},\boldsymbol{r_2})$ are the inverse Fourier transform of the centrally shifted spectra as described above in Eqs. (5.11-5.14) and contain only the information about the GSPs of the object field.

Now, substituting Eq. (5.3) in Eq. (5.4), the GSPs of the source are represented as

$$S_n^O(\boldsymbol{r_1},\boldsymbol{r_2}) = \sum_{a,b}\int\left\{\iint U_a^{O*}\left(\boldsymbol{\rho}_1\right)\sigma_{ab}^n U_b^O\left(\boldsymbol{\rho}_2\right)h^*(\boldsymbol{r_1}-\boldsymbol{\rho}_1)h(\boldsymbol{r_2}-\boldsymbol{\rho}_2)d^2\boldsymbol{\rho}_1 d^2\boldsymbol{\rho}_2\right\}d^2\boldsymbol{r_1}, \tag{5.22}$$

Putting the expression of $h(\boldsymbol{r}-\boldsymbol{\rho})$, making use of the relation $\int \exp\left(-\frac{ik}{z}[\boldsymbol{r_1}.(\boldsymbol{\rho_2}-\boldsymbol{\rho}_1)]\right) d^2\boldsymbol{r_1} \propto \delta(\boldsymbol{\rho_2}-\boldsymbol{\rho}_1)$, and Eq. (5.2), Eq. (5.2) transforms to [222]

$$S_n^O(\boldsymbol{r_1},\boldsymbol{r_2}) = \int S_n^O(\boldsymbol{\rho}) \exp\left(-\frac{ik}{z}\left[(\boldsymbol{r_2}-\boldsymbol{r_1}).\boldsymbol{\rho}\right]\right) d^2\boldsymbol{\rho}, \tag{5.23}$$

Eq. (5.23) is the vectorial van-Cittert Zernike (vCZ) theorem, which connects the source polarimetric parameters with the measured GSPs.

The SOP of the source is quantitatively represented by mapping the polarization ellipse in terms of SPs from Eq. (5.23). The orientation angle $\left(\psi(\boldsymbol{\rho})\right)$ and ellipticity angle $\left(\chi(\boldsymbol{\rho})\right)$ for the polarization ellipse are obtained as [27]

$$\psi(\boldsymbol{\rho}) = 0.5\, arctan\left(\frac{S_2^O(\boldsymbol{\rho})}{S_1^O(\boldsymbol{\rho})}\right), \qquad 0 \le \psi(\boldsymbol{\rho}) \le \pi \tag{5.24}$$

$$\chi(\boldsymbol{\rho}) = 0.5\, arcsin\left(\frac{S_3^O(\boldsymbol{\rho})}{S_0^O(\boldsymbol{\rho})}\right), \qquad -\frac{\pi}{4} \le \chi(\boldsymbol{\rho}) \le \frac{\pi}{4}. \tag{5.25}$$

5.3 Experiment

To experimentally validate our proposed approach, we designed an experimental setup to develop a single-shot polarimeter from random field analysis. The experimental setup, depicted in Fig. 5.2, comprises two sections: Part I represent a polarization state generator to confirm and check the performance of the proposed technique. At the same time, Part II focuses on a single-shot complete polarimetry. A detailed description of each part is explained here. A He-Ne laser (Thorlabs, HNL150L) emitting a vertically polarized beam with a wavelength of 632.8 nm is used as the light source. A half-wave plate (HWP) alters the incoming vertically polarized beam to a 45^0 linearly polarized beam. This diagonally polarized beam splits into two parts by a beam splitter (BS). The beam

transmitted from BS illuminates a phase-only spatial light modulator (SLM) (Pluto, Holoeye) with an 8 μm pixel pitch and a 1920 × 1080 pixels resolution. The object information displayed at the SLM is encoded in the horizontal polarization component, leaving the vertical polarization component unchanged. After reflection from the SLM, the SLM plane with a spatially varying polarization state is imaged at the ground glass (GG) plate (Thorlabs, DG20-120-MD) by a 4*f* imaging system composed of two lenses, L1 and L2, of equal focal lengths. This imaged beam with a defined polarization structure serves as a source $S_n^O(\boldsymbol{\rho})$ whose polarization state will be determined by our technique. A circular aperture (CA) with a 4 mm diameter is positioned before the SLM to control the object's size. On the other hand, the reflected beam from BS serves as the reference, creating an off-axis point source by introducing a tilt in the incoming beam using mirror M1, and focusing it on the GG plate through lens L2. These two sources, namely a beam from the SLM and a reference, illuminate different regions of the GG (as shown in the inset of Fig. 5.2) and generate random fields.

In Part II, the superposition of these independent fields is detected by a charge-coupled device (CCD) located at 200mm from the GG. We record the orthogonally polarized components of the superposed random field using a dual-channel polarization-sensitive geometry for single-shot Stokes polarimetry. This dual-channel geometry comprises a polarizing beam splitter (PBS) and two mirrors (M2 and M3) to separate the orthogonally polarized components of the scattered random field. After passing through the PBS, the transmitted x-polarized component and reflected y-polarized component travel nearly equal paths in counter-clockwise direction and are imaged at the CCD plane using a lens L3 arranged in a 2*f* configuration (*f*=200mm). The CCD camera (pco.pixelfly usb) has a resolution of 1392 × 1040 pixels and a pixel size 6.45 μm. The spatial separation of the

orthogonally polarized components ($I_{xx}(\boldsymbol{r}), I_{yy}(\boldsymbol{r})$) is adjusted via mirrors M2 and M3, enabling the simultaneous recording of the orthogonally polarized intensity patterns in a single-frame.

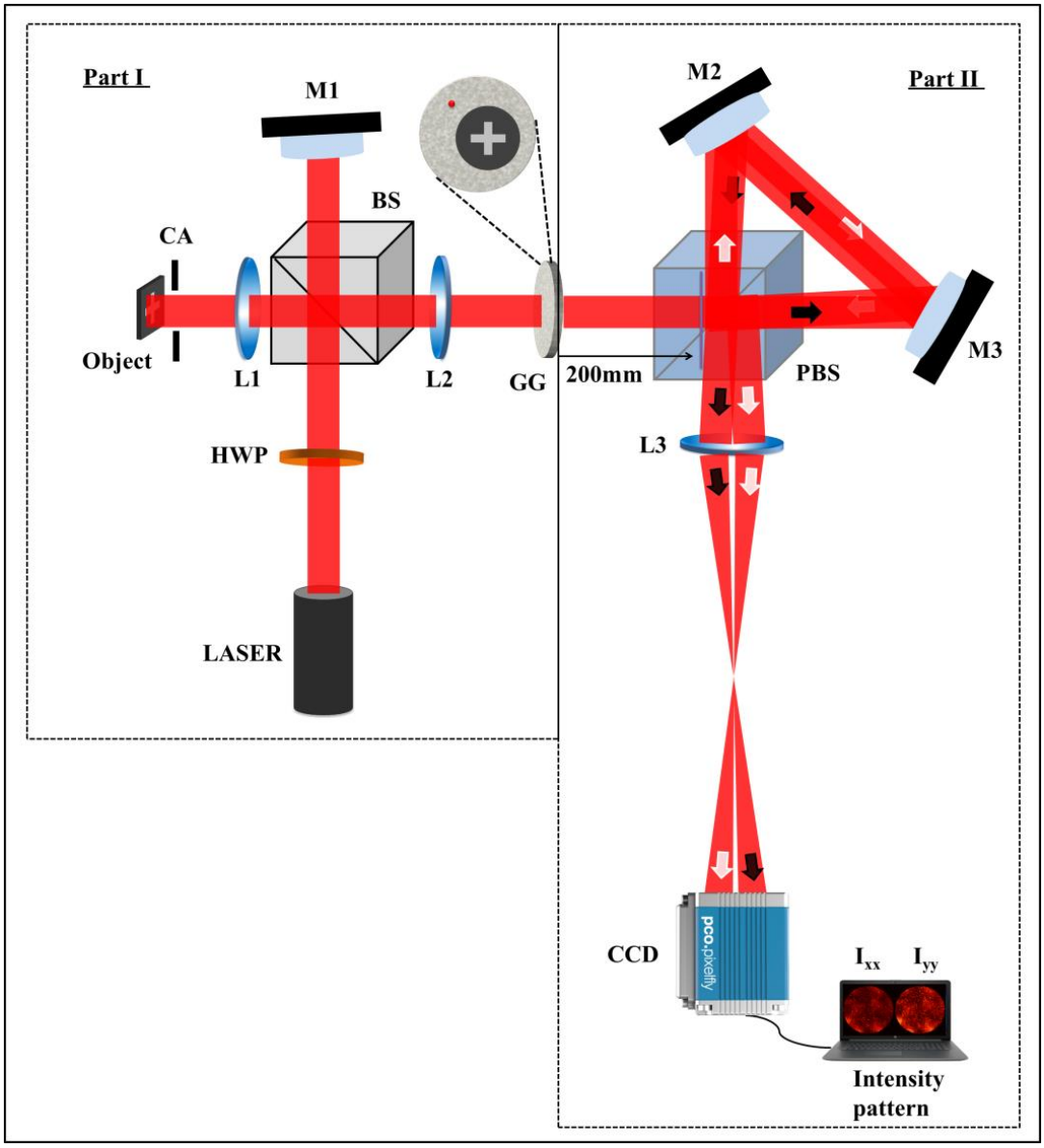

Fig. 5.2 represent an experimental configuration of the proposed technique. Laser: He-Ne laser, HWP: Half wave plate, BS: Beam splitter, SLM: Spatial light modulator, M1, M2, M3: Mirrors, L1, L2, L3: lenses, GG: Ground glass, CA: Circular Aperture, PBS: Polarizing beam splitter, CCD: Charge-coupled device. Violet dotted line plane is imaged on the CCD.

The captured intensity patterns are used to determine the first two SPs of the random fields at the recording plane as follows; $S_0(\boldsymbol{r}) = I_{xx}(\boldsymbol{r}) + I_{yy}(\boldsymbol{r})$ and $S_1(\boldsymbol{r}) = I_{xx}(\boldsymbol{r}) - I_{yy}(\boldsymbol{r})$. The correlation of fluctuations of these two SPs is digitally evaluated using Eq. (6). The two-point correlations of the recorded SPs provide $C_{00}(\Delta\boldsymbol{r}), C_{01}(\Delta\boldsymbol{r}), C_{10}(\Delta\boldsymbol{r}), C_{11}(\Delta\boldsymbol{r})$ and the GSPs, as explained in Eqns. (5.7)-(5.22). Hence, this technique is free from a QWP and LP and their mechanical rotations to recover the complex GSPs [221,222]. Finally, the four SPs of the source, i.e. $S_n^O(\boldsymbol{\rho})$, are retrieved from the GSPs as expressed in Eq. (5.23).

5.4 Simulation and experimental results

To test the efficacy of our polarimeter, we considered two polarization sources. For the first source, a "star" shaped phase object is introduced by the SLM. This object has a zero-phase star shape, while the background carries a π phase. Hence, in that 4mm beam, the star-shaped portion consists of the zero phases as displayed in SLM, while the remaining portion of the beam consists of the background phase as described above. For the second source, the plus-shaped feature consists of phase π/2 and a background with phase $3\pi/2$. For a diagonally polarized light incidence at the SLM, these modulations are loaded in the x-polarization component and y polarization component remains unmodulated.

Experimentally reconstructed full-Stokes parameters, $S_n^O(\boldsymbol{\rho})$ for both sources are shown in Fig. 5.3. The first row in Fig. 5.3 (a)-(d) corresponds to the four SPs for the first source. In this case, $S_0^O(\boldsymbol{\rho})$ and $S_2^O(\boldsymbol{\rho})$ are non-zero over the beam size, consistent with the phase information of the object and $S_1^O(\boldsymbol{\rho})$ and $S_3^O(\boldsymbol{\rho})$ are nearly zero. Similarly, the second row in Fig. 5.3 (e)-(h) depicts the four SPs for the second source. In this case,

$S_0^O(\boldsymbol{\rho})$ and $S_3^O(\boldsymbol{\rho})$ are non-zero over the beam, as expected for a $\pi/2$ phase difference between the orthogonal polarization components of equal amplitude and both $S_1^O(\boldsymbol{\rho})$ and $S_2^O(\boldsymbol{\rho})$ are zero.

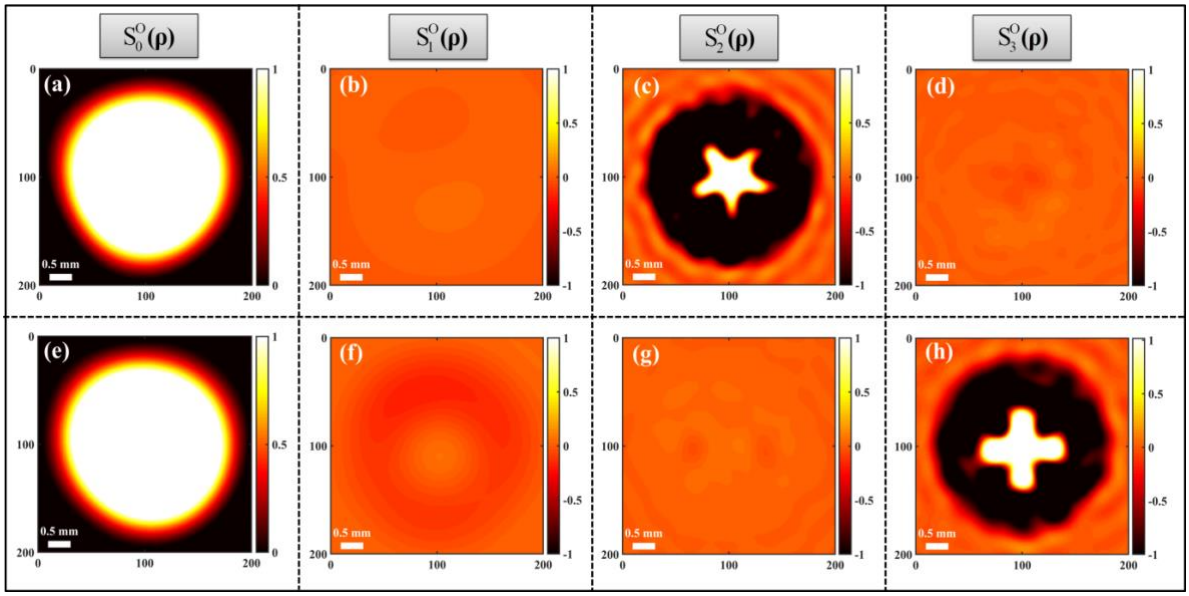

Fig. 5.3 Experimentally measured SPs of the source with different SOP. (a)-(b) shows the SPs for the "star", (e)-(h) represent the SPs for the "plus". Scale bar: 0.5 mm.

To quantitatively map the polarization state over the source, polarization ellipses are presented in Fig. 5.4 for both cases. The orientation angle and ellipticity are calculated, as represented in Eqs. (5.24, 5.25), for the polarization ellipse plots for these two sources. As depicted in Fig. 5.4(a), the star-shaped region shows a diagonal orientation. In contrast, the outer region exhibits an anti-diagonal linearly polarized orientation due to the π phase difference between the two regions. On the other hand, for the second source, as shown in Fig. 5.4(b), the polarization ellipse plot reveals right-circularly polarized (RCP) and left-circularly polarized (LCP) orientations, corresponding to plus and background regions of the beam, respectively, demonstrating a change in handedness.

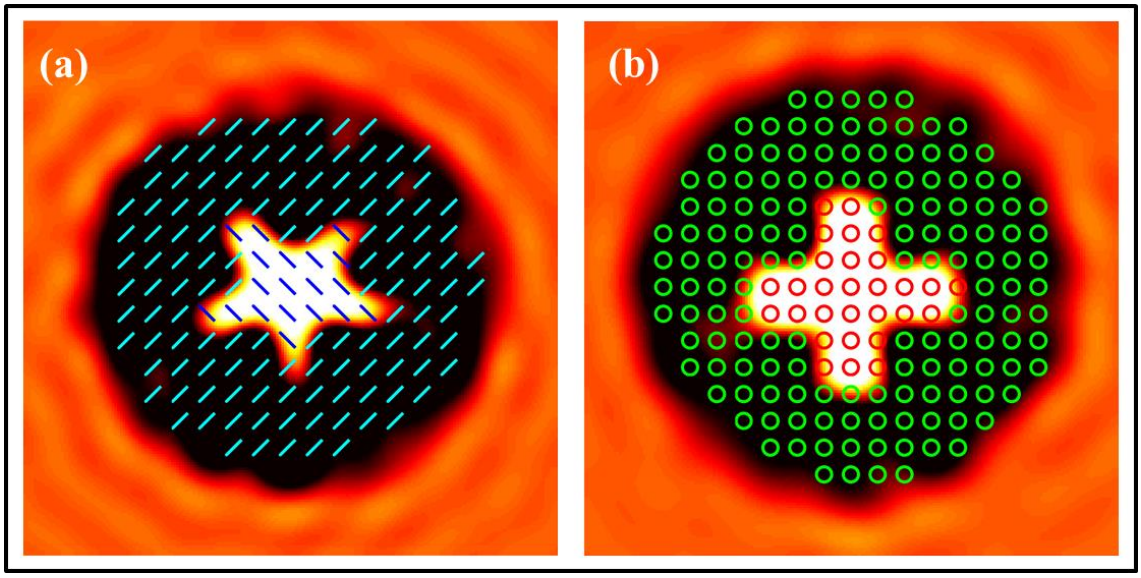

Fig. 5.4 (a), (b) represents the polarization ellipse plots of experimentally measured SPs for the two sources. 'Blue' and 'cyan' colors depict the orientations of 45^0 and -45^0 linearly polarized light, and 'red' and 'green' indicate the orientations of RCP and LCP light.

These errors are attributed to environmental noise, the small size of the polarization optics elements, the response of polarization-sensitive optics, the pixel resolution of CCD, etc. However, the error can be minimized using bigger-size polarization optics and a higher-resolution camera.

5.5 Conclusion

In this chapter, we have proposed and experimentally demonstrated a new single-shot quantitative full-Stokes polarimetry technique from the scattered random light. Two-point Stokes correlation of scattered random light enables the recovery of SOP of the incident light beam from the. Dual-channel recording of the two interferograms of orthogonal polarization components eliminates the need of mechanical rotation of polarization elements like QWP and LP. As a result, the complete SPs can be determined from a single intensity pattern. The feasibility of the proposed technique was validated through experimental measurements of the four SPs for two different sources and characterized by

polarization ellipse plots. The experimental results, showing good agreement with theoretical predictions for both linear and circular polarizations, confirm the accuracy of the technique in polarization detection. This experimental technique offers significant advantages for real-time Stokes polarimetry. It may be helpful in biomedical imaging, polarization imaging through scattering media, evaluating polarization dynamics, polarization-based communication systems, etc.